

2023-07-14

Constrained tropical land temperature-precipitation sensitivity reveals decreasing evapotranspiration and faster vegetation greening in CMIP6 projections

Zhu, B

<https://pearl.plymouth.ac.uk/handle/10026.1/21235>

10.1038/s41612-023-00419-x

npj Climate and Atmospheric Science

Springer Science and Business Media LLC

All content in PEARL is protected by copyright law. Author manuscripts are made available in accordance with publisher policies. Please cite only the published version using the details provided on the item record or document. In the absence of an open licence (e.g. Creative Commons), permissions for further reuse of content should be sought from the publisher or author.

1 **Constrained tropical land temperature-precipitation sensitivity reveals**
2 **decreasing evapotranspiration and faster vegetation greening in CMIP6**
3 **projections**

4

5 **Authors:** Boyuan Zhu^{1,2}, Yongzhou Cheng^{1,2}, Xuyue Hu^{1,2}, Yuanfang Chai^{3✉}, Wouter R. Berghuijs⁴,
6 Alistair G. L. Borthwick^{5,6}, Louise Slater⁷.

7 **Affiliations:**

8 1 School of Hydraulic and Environmental Engineering, Changsha University of Science &
9 Technology, Changsha 410114, China

10 2 Key Laboratory of Water-Sediment Sciences and Water Disaster Prevention of Hunan Province,
11 Changsha 410114, China

12 3 State Key Laboratory of Earth Surface Processes and Resource Ecology, Faculty of Geographical
13 Science, Beijing Normal University, Beijing 100875, China.

14 4 Department of Earth Sciences, Free University Amsterdam, Amsterdam 1081 HV, the Netherlands

15 5 School of Engineering, The University of Edinburgh, Edinburgh EH9 3JL, UK

16 6 School of Engineering, Computing and Mathematics, University of Plymouth, Plymouth PL4 8AA,
17 UK

18 7 School of Geography and the Environment, University of Oxford, Oxford OX1 3QY, UK

19

20

21 email: yuanfangchai@163.com

22

23 **Abstract:** Over the tropical land surface, accurate estimates of future changes in temperature,
24 precipitation and evapotranspiration are crucial for ecological sustainability, but remain highly
25 uncertain. Here we develop a series of emergent constraints (ECs) by using historical and future
26 outputs from the Coupled Model Inter-comparison Project Phase 6 (CMIP6) Earth System Models
27 under the four basic Shared Socio-economic Pathway scenarios (SSP126, SSP245, SSP370, and
28 SSP585). Results show that the temperature sensitivity to precipitation during 2015-2100, which
29 varies substantially in the original CMIP6 outputs, becomes systematically negative across SSPs
30 after application of the EC, with absolute values between $-1.10\text{ }^{\circ}\text{C mm}^{-1}\text{ day}$ and $-3.52\text{ }^{\circ}\text{C mm}^{-1}\text{ day}$,
31 and with uncertainties reduced by 9.4% to 41.4%. The trend in tropical land-surface
32 evapotranspiration, which was increasing by 0.292 mm yr^{-1} in the original CMIP6 model outputs,
33 becomes significantly negative (-0.469 mm yr^{-1}) after applying the constraint. Moreover, we find a
34 significant increase of 58.7% in the leaf area index growth rate.

35 **Introduction**

36 Over the tropical land surface, a negative association between temperature and precipitation is
37 generally observed due to the cooling effect of land surface evapotranspiration, and is one of the
38 major processes between the earth and the atmosphere¹⁻³. However, future changes in these variables
39 under climate change remain highly uncertain. Thus, a robust evaluation of future changes in
40 temperature-precipitation-evapotranspiration and their interaction is necessary to assess the potential
41 resilience of tropical land areas to future climate change.

42 Previous studies have investigated current and future temperature, precipitation, and
43 evapotranspiration changes from regional to global scales, using Earth System Models from the
44 CMIP5 ensemble⁴⁻⁸. These studies were based on analyses of thermodynamic and dynamic responses

45 to changes in variables such as specific humidity and atmospheric circulation. Although the models
46 accommodate important processes, such as convection, aerosol effects, and land-atmosphere and
47 dynamic ocean-atmosphere interactions, the results show considerable spread⁹. The emergent
48 constraint (EC) method has recently been employed to reduce uncertainty in the model outputs, and
49 has led to significant improvement¹⁰⁻¹³. The constraint is typically built through a physically
50 explainable empirical linear regression between the inter-model spread in future estimates of
51 temperature/precipitation/evapotranspiration (i.e. their absolute value or their sensitivity to
52 controlling factors, defined as the dependent variable y) and historical values of variables (defined as
53 the independent variable x) produced by the CMIP5 ensemble^{10,11}. This relation can then be further
54 constrained by projecting observed values of x and their observational uncertainty (\pm one standard
55 deviation, denoted as SD) onto the y -axis through the empirical linear relationship^{10,11}, as the
56 observed values are likely to be sufficiently reliable to provide an accurate mean state of x . This
57 approach provides more reliable values of y with expectably narrower uncertainty¹⁰⁻¹².

58 CMIP6, the latest generation of CMIP, has finer horizontal-vertical resolutions and more
59 physically realistic representations of aerosol, cloud-radiation interaction, oceanic horizontal-vertical
60 mixing and convection, sea ice, and biogeochemical processes (e.g. carbon and nitrogen cycles) than
61 its predecessor, CMIP5^{10,14}. Recent works concerned with reproducing historical changes and
62 predicting future features in global temperature, precipitation, and evapotranspiration have
63 demonstrated that CMIP6 models provide projections that are more accurate and reliable than their
64 CMIP5 counterparts¹⁵⁻¹⁷.

65 Despite these improvements in CMIP6, there remains considerable uncertainty in the
66 projections of the sensitivity of future surface temperature to precipitation over the tropical land

67 surface, and the future growth rate of evapotranspiration and vegetation cover. CMIP models (and
68 constrained projections using the EC method) have projected a decline of the tropical forest,
69 especially in the Amazon, but the projection accuracy depends largely on the reliability of the
70 environmental variable projections^{12,18-23}. The tropical forest cover is closely related to factors such
71 as temperature, precipitation and evapotranspiration. As temperatures rise, the rates of plant
72 transpiration and respiration grow significantly due to amplified vegetation stomatal openings. This
73 intensification leads to substantial losses of water and CO₂ within plant bodies, subsequently causing
74 notable constraints in water use efficiency, photosynthesis and CO₂ fertilization which ultimately
75 suppress plant growth^{12,18-24}. Under decreasing precipitation, lower water availability is also
76 unfavorable for plant growth^{12,18-20,22-24}.

77 Here we assess the reliability of future projections of tropical land-surface
78 temperature-precipitation sensitivity, evapotranspiration and leaf area index (LAI). We first explore
79 the sensitivity of temperature to precipitation over the tropical land area within 23.5° S~23.5° N and
80 180° W~180° E. Our methodology is based on an emergent relationship established between the
81 future annual tropical land-surface temperature sensitivity to precipitation (dT/dP) and the historical
82 seasonal average dT/dP under the four basic SSP scenarios of CMIP6. The projected changes in
83 tropical land-surface temperature sensitivity are then employed to estimate absolute variations in
84 future tropical land-surface temperature, evapotranspiration and LAI.

85 **Results**

86 **Sensitivity of tropical land-surface temperature to precipitation**

87 It is widely acknowledged that the increasing atmospheric CO₂ concentration is the main
88 driving factor behind the significant warming of the Earth's surface²⁵⁻²⁸. However, interannual

89 oscillations in temperature may also be related to local precipitation changes, which has been
90 identified in the Amazon rainforest¹². Observed time series of annual land-surface temperature and
91 precipitation in the tropical zone from the HadCRUT4 dataset display oscillations roughly in
92 antiphase during the period of 1949 to 2005 (Fig. 1a). Negative associations are found at the annual
93 and seasonal scale between land-surface temperature and precipitation anomalies (Fig. 1b).
94 Supportive results are also derived from three other datasets (Supplementary Figures 1 and 2).

95 The underlying mechanism of the negative sensitivity of tropical land-surface temperature to
96 precipitation (i.e. opposite oscillations in Fig.1a and Supplementary Figure 1) is as follows:
97 increasing precipitation leads to more water availability in the soil and on the ground, enhancing the
98 cooling effect of evapotranspiration on sensible heating, and subsequently lowering the temperature
99 of the tropical land surface^{1,2,29}. This interpretation is supported by antiphase oscillations between
100 annual mean evapotranspiration and temperature on the tropical land surface (Fig.1c and
101 Supplementary Figure 3). Recent research also revealed that water availability (and especially
102 extreme drought) affects fluctuations of land-surface temperature in the tropical region, through
103 vegetation stomatal responses to the soil-moisture-deficit induced atmospheric water stress or the
104 plant metabolism downregulation³⁰. Moreover, as the dominant extreme climate event in controlling
105 matter-energy cycles between land surface and atmosphere over the tropical region, ENSO triggers
106 subsidence/rising weather systems and subsequently causes concurrent warming (cooling), decreased
107 (increased) humidity, less (more) cloud cover, less (more) precipitation, lower (higher) evaporation
108 and less (more) soil moisture^{2,31-32}, strengthening the negative feedback between tropical
109 land-surface temperature and precipitation. Here, if we use a moving average approach to reduce
110 disturbance from climate oscillations (i.e. ENSO and other compensating effects)^{9,31-33}, we find that

111 the negative association between temperature and precipitation is further strengthened (Fig.1d,
112 Supplementary Figure 4 and Supplementary Figure 5).

113 An effective index for representing tropical land-surface temperature change due to
114 evapotranspiration arising from precipitation is the temperature sensitivity to precipitation (dT/dP , $^{\circ}\text{C}$
115 $\text{mm}^{-1}\text{ day}$). We select a total of 26 models under the four SSP scenarios from the CMIP6 ensemble,
116 which provide both the required historical (1949-2005) and future (2015-2100)
117 temperature/precipitation outputs (Supplementary Table 1). A large spread occurs in the CMIP6
118 scenario estimates of the absolute value of future annual dT/dP , as indicated by its considerable
119 variability, ranging from -1.52 to 1.06 $^{\circ}\text{C mm}^{-1}\text{ day}$ for SSP126, from -1.52 to 2.19 $^{\circ}\text{C mm}^{-1}\text{ day}$ for
120 SSP245, from -3.63 to 4.75 $^{\circ}\text{C mm}^{-1}\text{ day}$ for SSP370, and from -4.31 to 5.00 $^{\circ}\text{C mm}^{-1}\text{ day}$ for SSP585
121 (Fig. 1e). Since the feedback among temperature, precipitation and evapotranspiration is a key
122 process between the land surface and the atmosphere, such large uncertainties may lead to
123 comparable uncertainties in the cycle among water, carbon and energy on the tropical land¹².

124 Using evapotranspiration data from the GLEAM dataset during the period of 1980-2014, we
125 calculated the annual rates of increase in evapotranspiration from the tropical land surface in wet and
126 dry seasons (Jan. to Mar. and May to Jul., respectively), and found that the rate of increase was
127 significantly larger in the dry season than in the wet season (0.23% yr^{-1} vs. 0.11% yr^{-1} ,
128 Supplementary Figure 6). This difference is likely to be related to seasonal effect of absolute water
129 storage in the tropical land: in the wet season, water storage is large and reaches the upper limit of
130 evapotranspiration, meaning that evapotranspiration cannot increase appreciably as water storage
131 continues to increase; whereas in the dry season, water storage is scarce, and evapotranspiration is
132 markedly enhanced as the water storage increases³⁴. In summary, larger fluctuations in the

133 evapotranspiration-cooling effect occur in the dry season, which profoundly affects the oscillation in
134 tropical land-surface temperature. Observations show that the dry-season land-surface temperature
135 exhibits tighter negative correlation (i.e. higher absolute values of R) with precipitation than the
136 wet-season temperature (Fig. 1b, Supplementary Figure 2), implying that changes in dry-season
137 dT/dP values dominate the annual negative sensitivity of temperature to precipitation. Model results
138 reveal that the future annual dT/dP exhibits a high positive correlation with the future dry-season
139 dT/dP for all four emission scenarios ($0.49 \leq R \leq 0.81$, $P < 0.001$, Fig. 1f), suggesting that the spread
140 in future dry-season dT/dP (Supplementary Figure 7) will lead to a comparable spread in future
141 annual dT/dP . Therefore, we can expect to constrain the future annual dT/dP through establishing an
142 emergent relationship between the future annual dT/dP and the historical dry-season dT/dP . In fact, a
143 similar emergent constraint on future dT/dP has been identified in the Amazon rainforest¹².

144 **EC on future dT/dP based on the CMIP6 ensemble**

145 We observed significant linear regressions (along with their corresponding errors) between the
146 future annual and the historical dry-season average values of dT/dP for the four SSP scenarios (Fig. 2,
147 Supplementary Figure 8), based on the spread in the CMIP6 ensemble (Figs. 1e-f). Linear
148 regressions between future annual and historical wet-season average values of dT/dP have lower
149 values of R and higher P values (Supplementary Figure 9), and therefore are not used. The observed
150 dry-season average dT/dP (vertical black line) \pm one standard deviation (light blue rectangle) derived
151 from the HadCRUT4 dataset are then plotted for the four SSP scenarios (Fig. 2, Supplementary
152 Figure 8). These two steps together establish the ECs on future annual dT/dP for the four SSP
153 scenarios. Associated probability density functions (PDFs) after applying the ECs are then calculated
154 based on error intervals of both the observed historical dry-season average values and projected

155 future annual values of dT/dP , while PDFs without the ECs are directly obtained from the CMIP6
156 ensemble (Fig. 2, Supplementary Figure 8).

157 After application of the ECs, the spreads of the PDFs under the four SSP scenarios become
158 compressed, revealing large reductions in uncertainty in future annual dT/dP compared with the
159 values directly derived from the CMIP6 ensemble. The reductions are 9.4%, 16.1%, 29.8%, and
160 41.4% for the four SSPs, respectively (Fig. 2, Supplementary Figure 8). Importantly, the best
161 estimates of the constrained future annual dT/dP (each corresponding to the peak in the PDF) exhibit
162 large decreases from pre-EC to post-EC conditions (Fig. 2, Supplementary Figure 8, Supplementary
163 Table 2). Pre-EC values of the best estimates of dT/dP are $-0.14\text{ }^{\circ}\text{C mm}^{-1}\text{ day}$, $-0.27\text{ }^{\circ}\text{C mm}^{-1}\text{ day}$,
164 $0.57\text{ }^{\circ}\text{C mm}^{-1}\text{ day}$, and $1.03\text{ }^{\circ}\text{C mm}^{-1}\text{ day}$, respectively, under the four SSP scenarios (Fig. 2,
165 Supplementary Figure 8, Supplementary Table 2), suggesting uncertainty even in the sign of future
166 annual dT/dP , if different SSP scenarios are used. However, the post-EC values drop to $-1.10\text{ }^{\circ}\text{C}$
167 $\text{mm}^{-1}\text{ day}$, $-1.63\text{ }^{\circ}\text{C mm}^{-1}\text{ day}$, $-2.86\text{ }^{\circ}\text{C mm}^{-1}\text{ day}$, and $-3.52\text{ }^{\circ}\text{C mm}^{-1}\text{ day}$, respectively, with the
168 absolute decreases reaching $0.96\text{ }^{\circ}\text{C mm}^{-1}\text{ day}$, $1.36\text{ }^{\circ}\text{C mm}^{-1}\text{ day}$, $3.43\text{ }^{\circ}\text{C mm}^{-1}\text{ day}$, and $4.55\text{ }^{\circ}\text{C}$
169 $\text{mm}^{-1}\text{ day}$, correspondingly (Fig. 2, Supplementary Figure 8, Supplementary Table 2), meaning that
170 future annual dT/dP becomes systematically negative across all SSP scenarios. Decreases from
171 pre-EC to post-EC conditions are therefore conspicuous. PDFs based on the three other observational
172 datasets also demonstrate reductions in both the uncertainty and the best estimate (Supplementary
173 Figure 10).

174 Out-of-sample testing is an effective way to assess whether these emergent relationships have
175 emerged solely by chance¹⁰. Using 25 CMIP5 models, we still find a tight relationship between
176 future annual dT/dP and historical dry-season dT/dP under the RCP2.6 scenario ($R=0.64$, $P<0.001$,

177 Supplementary Figure 11). When driving the relationship with the observations, the constraint also
178 shifts the future annual dT/dP from -0.89 ± 0.79 °C mm⁻¹ day to a more negative value of $-1.43 \pm$
179 0.65 °C mm⁻¹ day. This testing further supports the reliability of our introduced emergent constraint.

180 **Future evapotranspiration from tropical land**

181 Evapotranspiration from tropical land depends strongly on variations in tropical land
182 temperature and precipitation, as is illustrated by the strong positive correlation between the future
183 annual growth rate in evapotranspiration and the future annual dT/dP under the high emission
184 scenario of SSP585 (Fig. 3a). By projecting the post-EC value of future annual $dT/dP \pm$ one standard
185 deviation (vertical black line \pm light blue rectangle) onto the y-axis through the linear regression
186 relation (with forecast error), we find that evapotranspiration is likely to experience a reduction at a
187 rate of -0.469 ± 0.430 mm yr⁻¹ under SSP585 during 2015-2100 (Fig.3a). Conversely, under pre-EC
188 conditions, an increasing rate of evapotranspiration of 0.292 ± 0.533 mm yr⁻¹ is projected,
189 corresponding to the peak of the pre-EC PDF curve (Fig. 3b). In other words, after application of the
190 EC, evapotranspiration from tropical land is projected to decrease substantially in the future under
191 the high emission scenario of SSP585. Moreover, the PDF curve corresponding to the future annual
192 trend in tropical land evapotranspiration shows a notable narrowing from pre-EC to post-EC
193 conditions, suggesting a reduction of 19.3% in uncertainty of the projection (Fig. 3b).

194 Past research suggests a significant decline in soil water content in the tropics accompanied by
195 an expected rise in aridification³⁵. This would result in the soil's water supply becoming inadequate
196 to meet the increasing evaporative demand from the atmosphere. This may be the reason for the
197 decrease in future tropical evapotranspiration. A similar feedback between soil water and
198 evapotranspiration has been reported which suggested that the observed decline of global

199 evapotranspiration during 1998-2008 was primarily driven by moisture shortage in the Southern
200 Hemisphere³⁶.

201 **Future vegetation greening on tropical land**

202 Temperature and precipitation are key climatic factors that affect vegetation dynamics on the
203 tropical land, as is confirmed by the strong relationship between the future annual growth rate in
204 tropical land LAI and future annual dT/dP across CMIP6 models under the SSP585 scenario
205 ($R=-0.82$, $P<0.001$, Fig.4a). The relationship indicates that a more negative dT/dP (i.e., a higher
206 evaporative cooling effect) after application of the EC is associated with greater greening of tropical
207 vegetation. Hence, the overestimate of future dT/dP by the original CMIP6 models implies that they
208 equally underestimated the increase in tropical land vegetation. The original CMIP6 models
209 projected a future annual growth rate in LAI of $0.0085 \pm 0.0073 \text{ m}^2 \text{ m}^{-2} \text{ yr}^{-1}$ under the SSP585
210 scenario (Fig. 4b). However, after applying the constraint (Fig. 4a), the future tropical land LAI is
211 expected to increase by $0.0205 \pm 0.0065 \text{ m}^2 \text{ m}^{-2} \text{ yr}^{-1}$, demonstrating that the raw CMIP6 models
212 underestimated the future increasing trend in tropical land LAI by 58.7% under the SSP585 scenario
213 (Fig. 4b).

214 When there is enough water in the soil to meet the transpiration demand, the increase in the LAI
215 growth rate typically strengthens the process of transpiration, and results in higher evapotranspiration.
216 The counterintuitive downward trend in the tropical land evapotranspiration (Fig. 3) might be related
217 to the change in soil water content. Under the high emission scenario of SSP585, more than half of
218 the earth's land surface is likely to experience a severe limitation in future soil water content³⁵, which
219 would exert an inhibitory effect on the tropical land evapotranspiration, as is supported by the
220 positive correlation between the soil water content and evapotranspiration in Supplementary Figure

221 12. If this kind of mechanism overwhelms the positive effect of LAI growth, decrease in
222 evapotranspiration can be expected.

223 **Discussion**

224 We define the wet and dry seasons over the tropical land surface as May to July and January to
225 March, respectively, in this study. We first exclude the subareas different from the whole tropical
226 land area in which dry-season months are defined as May to July. These subareas are rain-less and
227 desert regions. EC method is then applied to the remaining area and the constrained result is found to
228 be quite similar to that of the whole tropical land area, with the discrepancy of merely 14.5-19.3%
229 (Supplementary Figure 13). We then establish emergent relationships between historical monthly
230 dT/dP and future annual dT/dP , as in Thackeray et al. (2019)³⁹, and find that the relationships are
231 most significant for the defined dry-season months (i.e. May to Jul.) (Supplementary Figure 14),
232 which also leads to the largest uncertainty reductions for the constrained future annual dT/dP .

233 We use historical dry season dT/dP to constrain the future annual dT/dP over the tropical land.
234 We contend the plausible mechanism underpinning this emergent relationship is related to the
235 evaporative cooling effect: increased precipitation leads to more water availability on the ground and
236 in the soil, enhancing the cooling effect of evapotranspiration on sensible heating, and subsequently
237 lowering the temperature of the tropical land surface, leading to a negative value of dT/dP ^{1,2,29}. This
238 is supported by the antiphase oscillation between annual mean evapotranspiration and temperature
239 over the tropical land (Fig.1c, Supplementary Figure 3). A model with a high evaporative cooling
240 effect tends to produce a more negative dT/dP in both the historical and future periods, and vice
241 versa. The inter-model spread in both the historical dry season dT/dP and the future annual dT/dP are
242 dependent on the same evaporative cooling mechanism, which supports the existence of an emergent

243 relationship between them. As noted by Hall et al. (2019)¹⁰, verification of the mechanism
244 underpinning the emergent relationship is most straightforward and effective when the same physical
245 feedback process involves both the predictor and the predictand, and the only difference is the time
246 scale over which the process occurs. Hence, an emergent constraint that focuses on the projection of
247 a variable onto itself (i.e. the historical dry season dT/dP onto the future annual dT/dP in our case) is
248 most straightforward and reliable.

249 In Figure 2b, there is a striking change in dT/dP (i.e. $1.03\text{ }^{\circ}\text{C mm}^{-1}\text{ day}$ to $-3.52\text{ }^{\circ}\text{C mm}^{-1}\text{ day}$)
250 after applying the EC method. From Figure 2a, we see that modeled results of both historical dry
251 season dT/dP and future annual dT/dP show a large spread across the 26 CMIP6 models, rather than
252 biases from individual models, and the collection of data points forms the emergent relationship. If
253 we eliminate the handful of models with negative values of future annual dT/dP , the emergent
254 relationship still exists and changes little. The major driving factor for the significant shift in the
255 future annual dT/dP from pre-EC to post-EC conditions is the observed historical dry season dT/dP
256 (black vertical line), which is smaller than all the modeled values and results in the strongly negative
257 value of future annual dT/dP when substituting the observation into the emergent relationship (i.e.
258 the red regression line in Fig. 2a). This in turn highlights the high uncertainty of the CMIP model
259 simulations and the efficiency of the EC method. We can also see from Supplementary Table 2 that
260 the observed historical dry season dT/dP values of the four datasets and the corresponding post-EC
261 future annual dT/dP are all negative, and the changes from pre-EC to post-EC results are comparable
262 with the result shown in Figure 2, further supporting the method and conclusions of our study.

263 The Amazonian forest loss is projected to cross a tipping point and becomes increasingly severe
264 as future annual $\Delta T/\Delta P$ decreases¹², whereas the tropical LAI growth rate in this study experiences

265 an obvious increase as future annual dT/dP declines (Fig. 4). This divergent behavior can be
266 explained by different climate characteristics in these two regions. In the Amazon, precipitation is
267 abundant and has experienced a limited decrease (see Fig. 1a in Chai et al., 2021¹²); more negative
268 dT/dP indicates more temperature warming, which is unfavorable for vegetation growth due to
269 limitations in water use efficiency, photosynthesis and CO₂ fertilization^{12,18-24}. This demonstrates that
270 the Amazonian forest cover is mainly controlled by temperature. Nevertheless, the whole tropical
271 land surface, assessed in this work, contains a wide variety of subareas, including both arid deserts
272 and humid rainforests, where precipitation and temperature have respectively witnessed obvious
273 decreases and increases (see Fig. 1a in this study). Over this broader area, a more negative dT/dP
274 (namely the more negative linear regression slope in Fig. 1b in this study) means a lesser decrease in
275 precipitation for a given increase in temperature (it can be seen from Fig. 1a that the increasing rate
276 in temperature is roughly stable after 1975 whereas the decreasing rate in precipitation slowed from
277 1975-1992 to 1992-2005), which is favorable for vegetation growth due to higher water
278 availability^{12,18-20,22-24}. Recognition of the key environmental variables driving the two different
279 spatial-scale vegetation greenings is quite instructive for ecological preservation.

280 Apart from future annual dT/dP , we find that the historical LAI change also has a significant
281 emergent relationship with the future LAI trend across CMIP6 models (Supplementary Figure 15a).
282 After combining this EC with the observation of LAI ($0.0069 \text{ m}^2 \text{ m}^{-2} \text{ yr}^{-1}$), we estimate that the
283 constrained future annual growth rate in LAI is most likely to reach $0.0192 \text{ m}^2 \text{ m}^{-2} \text{ yr}^{-1}$, which is
284 quite consistent with the result ($0.0205 \text{ m}^2 \text{ m}^{-2} \text{ yr}^{-1}$) obtained by using the constrained future annual
285 dT/dP , with a discrepancy is only of 6.3%. These two equivalent results further improve the
286 reliability of the finding in this study. In contrast, historical changes of evapotranspiration,

287 temperature and precipitation show insignificant relationships with future LAI and
288 evapotranspiration variations (Supplementary Figure 15(b-f)).

289 Existing emergent constraint-based findings^{13,39-44} are uniformly based on the assumption of the
290 same plausible mechanism underpinning the inter-model spreads in both the historical and future
291 changes for a certain environmental variable. This is the reason why all the previous studies^{38-40,45}
292 use a linear emergent relationship to reduce the prediction uncertainty in future variables. Similarly,
293 in this study, our emergent constraint focuses on the projection of a variable onto itself (i.e. the
294 historical dT/dP onto the future dT/dP), which involves in the same physical mechanism for both the
295 predictor and the predictand. Thus, a linear emergent relationship is a more reasonable selection.

296 One limitation of this study is related to the uncertainty of the observational datasets. Different
297 datasets exhibit a discrepancy in estimating the observed dT/dP , which may affect the post-EC
298 results. Considering a range of observational datasets might be an effective way to relieve this
299 influence. Here, we adopt four widely used datasets and find that the pre-EC dT/dP values are the
300 same under a given SSP scenario, the post-EC dT/dP values are consistently negative, and the
301 negative post-EC dT/dP values are comparable under a given SSP scenario (Supplementary Table 2),
302 which confirms the reliability of our findings. Furthermore, another synthetic method, termed the
303 Hierarchical Emergent Constraint (HEC) framework⁴⁶, also provides a practical pattern for
304 constraining the future climate projections, given that it incorporates the present-future climate
305 correlation, the bias between observations and ensemble mean, and the observation uncertainty. After
306 using this method, we find that the constrained future annual dT/dP remains virtually unchanged (i.e.
307 $-0.98\text{ }^{\circ}\text{C mm}^{-1}\text{ day}$ under SSP126, $-1.49\text{ }^{\circ}\text{C mm}^{-1}\text{ day}$ under SSP245, $-2.51\text{ }^{\circ}\text{C mm}^{-1}\text{ day}$ under
308 SSP370 and $-3.05\text{ }^{\circ}\text{C mm}^{-1}\text{ day}$ under SSP585) compared with the results seen in Supplementary

309 Table 2 (i.e. $-1.10\text{ }^{\circ}\text{C mm}^{-1}$ day under SSP126, $-1.63\text{ }^{\circ}\text{C mm}^{-1}$ day under SSP245, $-2.86\text{ }^{\circ}\text{C mm}^{-1}$ day
 310 under SSP370 and $-3.52\text{ }^{\circ}\text{C mm}^{-1}$ day under SSP585), with a discrepancy of merely 8.6-13.4%,
 311 which further improves the reliability of our main findings.

312 **Methods**

313 **Average values.** Values of temperature, precipitation, evapotranspiration and LAI are taken directly from the
 314 relevant datasets (see Data Availability). All values are at the grid scale, bounded in the geographic land area within
 315 $23.5^{\circ}\text{ S}\sim 23.5^{\circ}\text{ N}$ and $180^{\circ}\text{ W}\sim 180^{\circ}\text{ E}$. Spatial averages are obtained over the tropical land area. Herein, dT/dP is
 316 the rate of change of tropical land-surface average temperature with respect to tropical land-surface average
 317 precipitation. Changes in evapotranspiration and LAI are also derived from corresponding spatial averages.

318 **Linear regression and forecast error.** A linear regression is performed between x (independent variable) and y
 319 (dependent variable) using the least squares method⁶. That is, the best fit line corresponds to the minimum
 320 quadratic sum of the normal distances between the data points and the fitted line. Then, the best-estimate value of y
 321 (y_p) for a given value of x (x_p) is obtained by substituting x_p into the regression equation of the fit line^{6,12-13}.

322 The forecast error of y_p at x_p is estimated as:

323

$$\sigma(y_p) = s \sqrt{1 + \frac{1}{N} + \frac{(x_p - \bar{x})^2}{N \cdot \sigma_x^2}} \quad (1)$$

324 where N is the number of samples, \bar{x} is the geometric average across all elements in the independent variable
 325 sample, σ_x is the variance of x , and s is used to minimize the quadratic sum of the vertical distances during the
 326 linear regression analysis. σ_x and s are respectively calculated as follows:

327

$$\sigma_x = \sqrt{\sum_{i=1}^N (x_i - \bar{x})^2} \quad (2)$$

328

$$s^2 = \min\left(\frac{1}{N-2} \sum_{i=1}^N (y_{pi} - y_i)^2\right) \quad (3)$$

329 where x_i and y_i are the i -th elements in samples of the independent and dependent variables, and y_{pi} is the value of

330 y_p on the best fit line corresponding to y_i .

331 In Figs. 2(a), 3(a), and 4(a), and Supplementary Figure 7(a, c, e) and 10(a), x represents the historical dry season
332 dT/dP and future annual dT/dP , respectively, and y represents future annual dT/dP , future change in tropical land
333 evapotranspiration, and future annual growth rate in tropical land LAI, separately. Meanwhile, the observed dry
334 season average dT/dP (vertical black line) \pm one standard deviation (light blue rectangle) in Fig. 2(a) and
335 Supplementary Figure 7(a, c, e) and 10(a) are also determined using a linear regression process, in which the best
336 estimate (i.e. the vertical black line) is the slope of the linear regression line between observed historical dry season
337 T and observed historical dry season P , and a single standard deviation (i.e. the light blue rectangle) is calculated by
338 equation (1). Subsequently, the constrained future annual dT/dP (vertical black line) \pm one standard deviation (light
339 blue rectangle) in Figs. 3(a) and 4(a) are obtained by projecting the best estimate of historical dry season dT/dP
340 onto the red regression line and the orange shaded area in Fig. 2(a).

341 **PDFs.** Following Cox et al. (2018)⁶ and Chai et al. (2021)¹², PDFs of pre-EC values of dependent variables are
342 directly calculated from:

$$343 \quad P(y) = \frac{1}{\sqrt{2\pi\sigma(y_p)^2}} \exp\left[-\frac{(y - y_p)^2}{2\sigma(y_p)^2}\right] \quad (4)$$

344 By comparison, post-EC values (y') are constrained by dataset observations, and the corresponding PDFs are
345 determined from:

$$346 \quad P(y') = \int_{-\infty}^{+\infty} P(y)P(x')dx' \quad (5)$$

347 where x' represents the independent variable derived from observed datasets rather than the model results.

348 **Hierarchical Emergent Constraint (HEC) framework**

349 The hierarchical emergent constraint method requires data for the projected future climate variable (y),
 350 alongside simulated and observed current climate variables (x and x_0). Least-squares linear regression is applied to
 351 establish the emergent relationship between x and y :

$$352 \quad y = k(x - \bar{x}) + \bar{y} \quad (6)$$

353 where k is the regression coefficient, which can be calculated by using equation (7); \bar{x} and \bar{y} are the model
 354 ensemble mean values of x and y .

$$355 \quad k = \rho \frac{\sigma_y}{\sigma_x} \quad (7)$$

356 where ρ is the correlation coefficient between x and y , and σ_x and σ_y are standard deviations of x and y across the
 357 CMIP6 models.

358 If the emergent relationship is causal and significant, we can constrain y by combining with the observed
 359 current climate variable x_0 and its uncertainty. Assuming that the observation is related to the current climate
 360 through an additive-noise model under Gaussian assumptions, we use the signal-noise ratio (SNR) in x_0 to correct
 361 the scaling factor k (equation (8)). SNR defines the relative strength of the signal variability to the noise variability
 362 and is estimated by using equation (9), where σ_x^2 and σ_0^2 are variances across the models and across the different
 363 observation datasets. If the noise dominates the signal, the forecast anomaly will approach 0. Otherwise, if the
 364 signal drives the noise (i.e. $\text{SNR} \geq 1$), the correction through equation (8) has little effect, and thus the constrained
 365 future climate \bar{y}_0 with its standard deviation can be estimated by equations (10) and (11), respectively.

$$366 \quad k^* = \frac{1}{1 + \text{SNR}^{-1}} k \quad (8)$$

$$367 \quad \text{SNR} = \frac{\sigma_x^2}{\sigma_0^2} \quad (9)$$

$$368 \quad \bar{y}_0 = \bar{y} + \frac{k}{1 + \text{SNR}^{-1}} (\bar{x}_0 - \bar{x}) \quad (10)$$

$$369 \quad \sigma_y^2 = \left(1 - \frac{\rho^2}{1 + \text{SNR}^{-1}} \right) \sigma_y^2 \quad (11)$$

370 After using the HEC framework, the uncertainty of the projected future climate y_0 is reduced by $\frac{\rho^2}{1 + \text{SNR}^{-1}}$.

371 More detailed information of the HEC framework can be seen in Bowman et al. (2018)⁴⁶.

372 **Data Availability**

373 CMIP6 model simulations of monthly data of temperature/precipitation during 1949–2100, and evapotranspiration
374 and LAI during 2015–2100 under the emission scenarios of SSP126, SSP245, SSP370 and SSP585 were collected
375 from <https://esgf-node.llnl.gov/projects/cmip6/>. Observed monthly temperature and precipitation data during 1949–
376 2005 are derived from the HadCRUT4 (<http://www.cru.uea.ac.uk/>), GPCP
377 (<https://climatedataguide.ucar.edu/climate-data/gpcp-global-precipitation-climatology-centre>), NOAA
378 (<https://www.esrl.noaa.gov/psd/data/gridded/data.noaaglobaltemp.html>), GISS
379 (<https://www.esrl.noaa.gov/psd/data/gridded/data.gistemp.html>) and Delaware
380 (https://psl.noaa.gov/data/gridded/data.UDel_AirT_Precip.html) datasets. HadCRUT4 and Delaware provide both
381 temperature and precipitation data, whereas the GPCP dataset solely provides precipitation data, and NOAA and
382 GISS datasets only provide temperature data. Hence, we use HadCRUT4, Delaware, and combinations of
383 GISS+GPCP and NOAA+GPCP to establish the sensitivity of tropical land-surface temperature to precipitation in
384 this study. Observed monthly data of evapotranspiration during 1980–2014 were gathered from the GLEAM dataset
385 (<https://www.gleam.eu/>).

386 **Code Availability**

387 The code used to generate the results for this study is available upon reasonable request from the
388 corresponding author.

389 **Acknowledgements**

390 This work was supported by the National Natural Science Foundation of China (Grant No.
391 52209079), the Natural Science Foundation of Hunan Province (Grant No. 2021JJ40607), the

392 Scientific Research Foundation of Hunan Provincial Education Department (Grant No. 20B021), the
393 UK Natural Environment Research Council (NERC; Grants No. NE/S009000/1 and NE/S015728/1),
394 and UK Research and Innovation (Grant No. MR/V022008/1). We thank Prof. Han Dolman for his
395 constructive comments on an early version of this manuscript, especially with regard to the
396 expression of response sensitivity between temperature and precipitation, which contribute to
397 validity of this study and highly improve the quality of the manuscript.

398 **Author Contributions**

399 B. Y. Z. and Y. F. C. designed the research, led the writing and performed the data analysis; Y. Z. C.,
400 X. Y. H., W. R. B., A. G. L. B. and L. S. contributed to the structure and writing of each version of
401 the manuscript.

402 **Competing Interests**

403 The Authors declare no Competing Financial or Non-Financial Interests.

404 **References**

- 405 1. Trenberth, K. E. & Shea, D. J. Relationships between precipitation and surface temperature. *Geophys. Res. Lett.*
406 **32**, L14703 (2005).
- 407 2. Adler, R. F. *et al.* Relationships between global precipitation and surface temperature on interannual and longer
408 timescales (1979-2006). *J. Geophys. Res-Atmos.* **113**, D22104 (2008).
- 409 3. Wang, J. J., Adler, R. F. & Gu, G. J. Tropical rainfall-surface temperature relations using Tropical Rainfall
410 Measuring Mission precipitation data. *J. Geophys. Res-Atmos.* **113**, D18115 (2008).
- 411 4. Frierson, D. M. W. *et al.* Contribution of ocean overturning circulation to tropical rainfall peak in the Northern
412 Hemisphere. *Nat. Geosci.* **6**, 940-944 (2013).
- 413 5. Laine, A., Nakamura, H., Nishii, K. & Miyasaka, T. A diagnostic study of future evaporation changes projected

- 414 in CMIP5 climate models. *Clim. Dynam.* **42**, 2745-2761 (2014).
- 415 6. Cox, P. M., Huntingford, C. & Williamson, M. S. Emergent constraint on equilibrium climate sensitivity from
416 global temperature variability. *Nature* **553**, 319-322 (2018).
- 417 7. Jimenez-de-la-Cuesta, D. & Mauritsen, T. Emergent constraints on Earth's transient and equilibrium response
418 to doubled CO₂ from post-1970s global warming. *Nat. Geosci.* **12**, 902-905 (2019).
- 419 8. Feron, S., Cordero, R. R., Damiani, A. & Jackson, R. B. Climate change extremes and photovoltaic power
420 output. *Nat. Sustain.* **4**, 270-276 (2021).
- 421 9. Taylor, K. E., Stouffer, R. J. & Meehl, G. A. An overview of CMIP5 and the experiment design. *B. Am.*
422 *Meteorol. Soc.* **93**, 485-498 (2012).
- 423 10. Hall, A., Cox, P., Huntingford, C. & Klein, S. Progressing emergent constraints on future climate change. *Nat.*
424 *Clim. Change.* **9**, 269-278 (2019).
- 425 11. Chai, Y. F. *et al.* Constrained CMIP6 projections indicate less warming and a slower increase in water
426 availability across Asia. *Nat Commun* **13**, 4124 (2022).
- 427 12. Chai, Y. F. *et al.* Constraining Amazonian land surface temperature sensitivity to precipitation and the
428 probability of forest dieback. *npj. Clim. Atmos. Sci.* **4**, 6 (2021).
- 429 13. Shiogama, H., Watanabe, M., Kim, H. & Hirota, N. Emergent constraints on future precipitation changes.
430 *Nature* **602**, 612–616 (2022).
- 431 14. Chai, Y. F. *et al.* Using precipitation sensitivity to temperature to adjust projected global runoff. *Environ Res*
432 *Lett* **16**, 124032 (2021)
- 433 15. Papalexiou, S. M., Rajulapati, C. R., Clark, M. P. & Lehner, F. Robustness of CMIP6 historical global mean
434 temperature simulations: Trends, long-term persistence, autocorrelation, and distributional shape. *Earth's*
435 *Future* **8**, e2020EF001667 (2020).

- 436 16. Wang, Z. Z., Zhan, C. S., Ning, L. K. & Guo, H. Evaluation of global terrestrial evapotranspiration in CMIP6
437 models. *Theor. Appl. Climatol.* **143**, 521-531 (2021).
- 438 17. Zhu, Y. Y. & Yang, S. N. Interdecadal and interannual evolution characteristics of the global surface
439 precipitation anomaly shown by CMIP5 and CMIP6 models. *Int. J. Climatol.* **41**, E1100-E1118 (2021).
- 440 18. Cox, P. M. *et al.* Amazonian forest dieback under climate-carbon cycle projections for the 21st century. *Theor.*
441 *Appl. Climatol.* **78**, 137-156 (2004).
- 442 19. Imbach, P. *et al.* Modeling potential equilibrium states of vegetation and terrestrial water cycle of Mesoamerica
443 under climate change scenarios. *J. Hydrometeorol.* **13**, 665-680 (2012).
- 444 20. Drijfhout, S. *et al.* Catalogue of abrupt shifts in Intergovernmental Panel on Climate Change climate models. *P.*
445 *Natl. Acad. Sci. USA* **112**, E5777-E5786 (2015).
- 446 21. Cox, P. M. *et al.* Sensitivity of tropical carbon to climate change constrained by carbon dioxide variability.
447 *Nature* **494**, 341-344 (2013).
- 448 22. Alemayehu, T., van Griensven, A., Woldegiorgis, B. T. & Bauwens, W. An improved SWAT vegetation growth
449 module and its evaluation for four tropical ecosystems. *Hydrol. Earth Syst. Sc.* **21**, 4449-4467 (2017).
- 450 23. Berg, A. & Sheffield, J. Evapotranspiration Partitioning in CMIP5 Models: Uncertainties and Future
451 Projections. *J. Climate* **32**, 2653-2671 (2019).
- 452 24. Mendivelso, H. A., Camarero, J. J., Gutierrez, E. & Castano-Naranjo, A. Climatic influences on leaf phenology,
453 xylogenesis and radial stem changes at hourly to monthly scales in two tropical dry forests. *Agr. Forest*
454 *Meteorol.* **216**, 20-36 (2016).
- 455 25. Li, B. G. *et al.* The contribution of china's emissions to global climate forcing. *Nature*, **531**, 357-361 (2016).
- 456 26. Tokarska, K.B. & Gillett, N.P. Cumulative carbon emissions budgets consistent with 1.5 degrees C global
457 warming. *Nat. Clim. Change* **8**, 296–299 (2018).

- 458 27. Tong, D. *et al.* Committed emissions from existing energy infrastructure jeopardize 1.5 degrees C climate target.
459 *Nature* **572**, 373–377 (2019).
- 460 28. Fernandez-Martinez, M. *et al.* Global trends in carbon sinks and their relationships with CO₂ and temperature.
461 *Nat. Clim. Change* **9**, 73–79 (2019).
- 462 29. Muller, C. J. & O’Gorman, P. A. An energetic perspective on the regional response of precipitation to climate
463 change. *Nat. Clim. Change* **1**, 266-271 (2011).
- 464 30. Luo, X. Z. & Keenan, T. F. Tropical extreme droughts drive long-term increase in atmospheric CO₂ growth rate
465 variability. *Nat Commun* **13**, 1193 (2022).
- 466 31. Le, T. & Bae, D. H. Response of global evaporation to major climate modes in historical and future Coupled
467 Model Intercomparison Project Phase 5 simulations. *Hydrol. Earth Syst. Sc.* **24**, 1131-1143 (2020).
- 468 32. Le, T. & Bae, D. H. Causal Impacts of El Nino-Southern Oscillation on Global Soil Moisture Over the Period
469 2015-2100. *Earth’s Future* **10**, e2021EF002522 (2022).
- 470 33. Easterling, D. R. *et al.* Climate extremes: Observations, modeling, and impacts. *Science* **289**, 2068-2074
471 (2000).
- 472 34. Chen, X., Alimohammadi, N. & Wang, D. B. Modeling interannual variability of seasonal evaporation and
473 storage change based on the extended Budyko framework. *Water Resour. Res.* **49**, 6067-6078 (2013).
- 474 35. Cook, B. I. *et al.* Twenty-first century drought projections in the CMIP6 forcing scenarios. *Earth’s Future*, **8**,
475 UNSP e2019EF001461 (2020).
- 476 36. Jung, M. *et al.* Recent decline in the global land evapotranspiration trend due to limited moisture supply.
477 *Nature*. **467**, 951-954 (2010).
- 478 37. Lian, X. *et al.* Partitioning global land evapotranspiration using CMIP5 models constrained by observations.
479 *Nat. Clim. Change* **8**, 640–646 (2018).

- 480 38. Chai, Y. F. *et al.* Constrained CMIP6 projections indicate less warming and a slower increase in water
481 availability across Asia. *Nat. Commun.* **13**, 4124 (2022).
- 482 39. Thackeray, C. W. & Hall, A. An emergent constraint on future Arctic sea-ice albedo feedback. *Nat. Clim.*
483 *Change* **9**, 972-978 (2019).
- 484 40. Hall, A., & Qu, X. Using the current seasonal cycle to constrain snow albedo feedback in future climate change.
485 *Geophys. Res. Lett.* **33**, L03502 (2006).
- 486 41. Sherwood, S. C., Bony, S. & Dufresne, J. L. Spread in model climate sensitivity traced to atmospheric
487 convective mixing. *Nature* **505**, 37-42 (2014).
- 488 42. DeAngelis, A. M., Qu, X., Zelinka, M. D. & Hall, A. An observational radiative constraint on hydrologic cycle
489 intensification. *Nature* **528**, 249-253 (2015).
- 490 43. Wenzel, S., Cox, P. M., Eyring, V. & Friedlingstein, P. Projected land photosynthesis constrained by changes in
491 the seasonal cycle of atmospheric CO₂. *Nature* **538**, 499–501 (2016).
- 492 44. Terhaar, J., Kwiatkowski, L. & Bopp, L. Emergent constraint on Arctic Ocean acidification in the twenty-first
493 century. *Nature* **582**, 379-383 (2020).
- 494 45. Tokarska, K. B. *et al.* Past warming trend constrains future warming in CMIP6 models. *Sci. Adv.* **6**, eaaz9549
495 (2020).
- 496 46. Bowman, K. W., Cressie, N., Qu, X. & Hall, A. (2018). A hierarchical statistical framework for emergent
497 constraints: Application to snow-albedo feedback. *Geophys. Res. Lett.* **45**, 13050-13059 (2018).

498 **Figure captions**

499

500 **Fig. 1 Association between tropical land-surface temperature and precipitation using HadCRUT4**
501 **observations and CMIP6 outputs. a,** Observed time series of annual tropical land-surface temperature and
502 precipitation from 1949 to 2005. **b,** Observed relationship between tropical land-surface temperature and
503 precipitation anomalies at annual and seasonal timescales (anomalies are computed as the value of a variable in a
504 certain year minus the mean over the multi-year period of 1949-2005). **c,** Comparison between the two observed

505 yearly time series of tropical land-surface evapotranspiration from GLEAM dataset and temperature from
506 HadCRUT4 dataset during 1980-2005. **d**, Linear relationships between observed tropical land-surface temperature
507 and precipitation before and after using a moving average with the window length of 5 years. Linear relationships
508 corresponding to other window lengths are illustrated in Supplementary Figure 4, and correlation coefficients and
509 slope values (i.e., dT/dP) are provided in Supplementary Figure 5. **e**, Spreads of future annual dT/dP modeled under
510 the four SSP scenarios. **f**, Relationship between future annual and historical dry-season values of tropical land
511 dT/dP modeled under the four SSP scenarios.

512

513 **Fig. 2 EC on future annual dT/dP based on CMIP6 models under the SSP585 scenario.** **a**, The constraint
514 consists of a linear regression (with the associated error) between the future annual simulated dT/dP and historical
515 dry season simulated dT/dP (red line and orange shaded area); then the constrained data is computed by projecting
516 the observed historical dry season $dT/dP \pm$ one standard deviation (vertical black line and light blue rectangle,
517 obtained from the HadCRUT4 dataset) onto the regression. **b**, Blue and grey lines are PDFs for the constrained
518 (post-EC) and unconstrained (pre-EC) future annual dT/dP , showing the change in projection uncertainty and the
519 best estimate of future annual dT/dP .

520

521 **Fig. 3 EC on future annual growth rate in tropical land evapotranspiration based on CMIP6 models (see**
522 **Supplementary Table 1) under the SSP585 scenario.** **a**, The constraint consists of a linear regression (with the
523 associated forecast error) between the future annual dT/dP and future annual growth rate in evapotranspiration (red
524 line and orange shaded area); the constrained data is computed by projecting the constrained future annual $dT/dP \pm$
525 one standard deviation (SD, vertical black line \pm light blue rectangle) onto the regression. **b**, Blue and grey lines are
526 PDFs for the constrained (post-EC) and unconstrained (pre-EC) future annual growth rates in evapotranspiration.
527 Note: The use of a constrained future variable (x) to constrain another future variable (y) has also been applied in
528 previous studies³⁷⁻³⁸. The logic is as follows: A tight interdependence (i.e. emergent relationship) is first found
529 between x and y based on originally modeled results. The constrained x is then applied in the emergent relationship
530 to obtain a more precise y given that this kind of x shows a much lower uncertainty.

531

532 **Fig. 4 EC on future annual growth rate in tropical land LAI based on CMIP6 models (see Supplementary**
533 **Table 1) under the SSP585 scenario.** **a**, The constraint consists of a linear regression (with the associated forecast
534 error) between the future annual dT/dP and future annual growth rates in tropical land LAI (red line and orange
535 shaded area); the constrained data is computed by projecting the constrained future annual $dT/dP \pm$ one standard
536 deviation (SD, vertical black line \pm light blue rectangle) onto the regression. **b**, Blue and grey lines are PDFs for the
537 constrained (post-EC) and unconstrained (pre-EC) future annual growth rates in tropical land LAI.

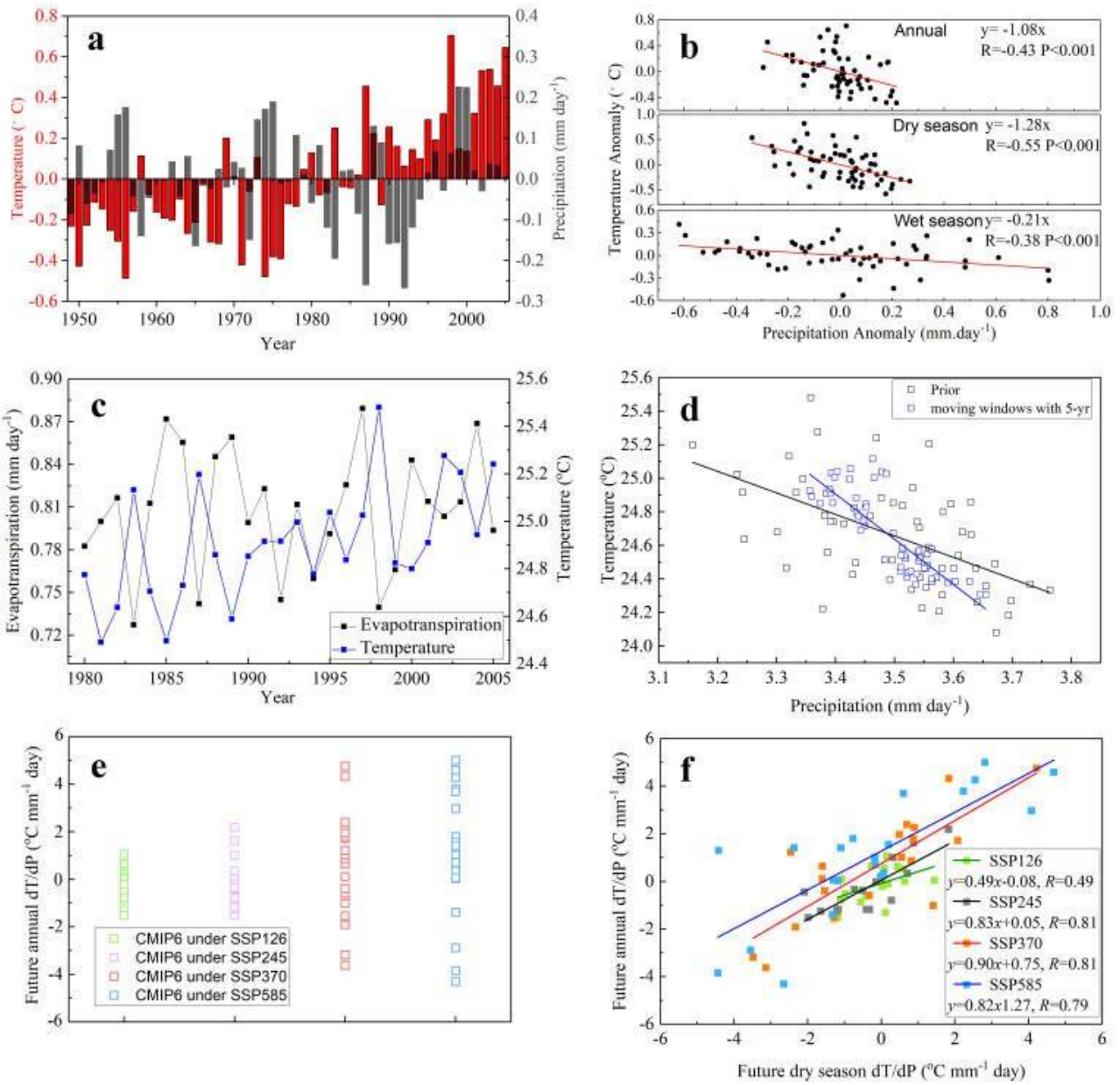
538

539

540

541

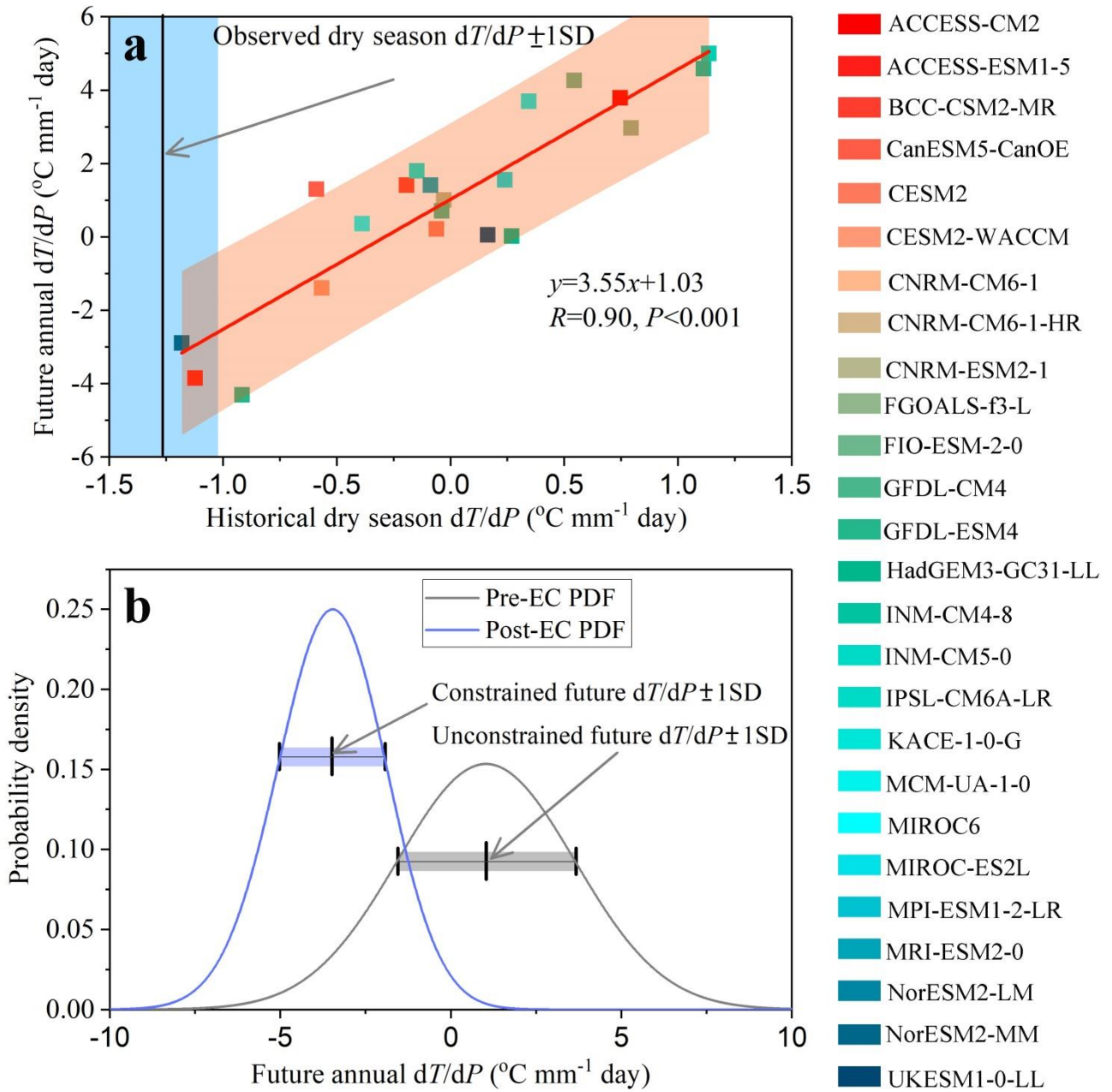
542 **Fig. 1**



543

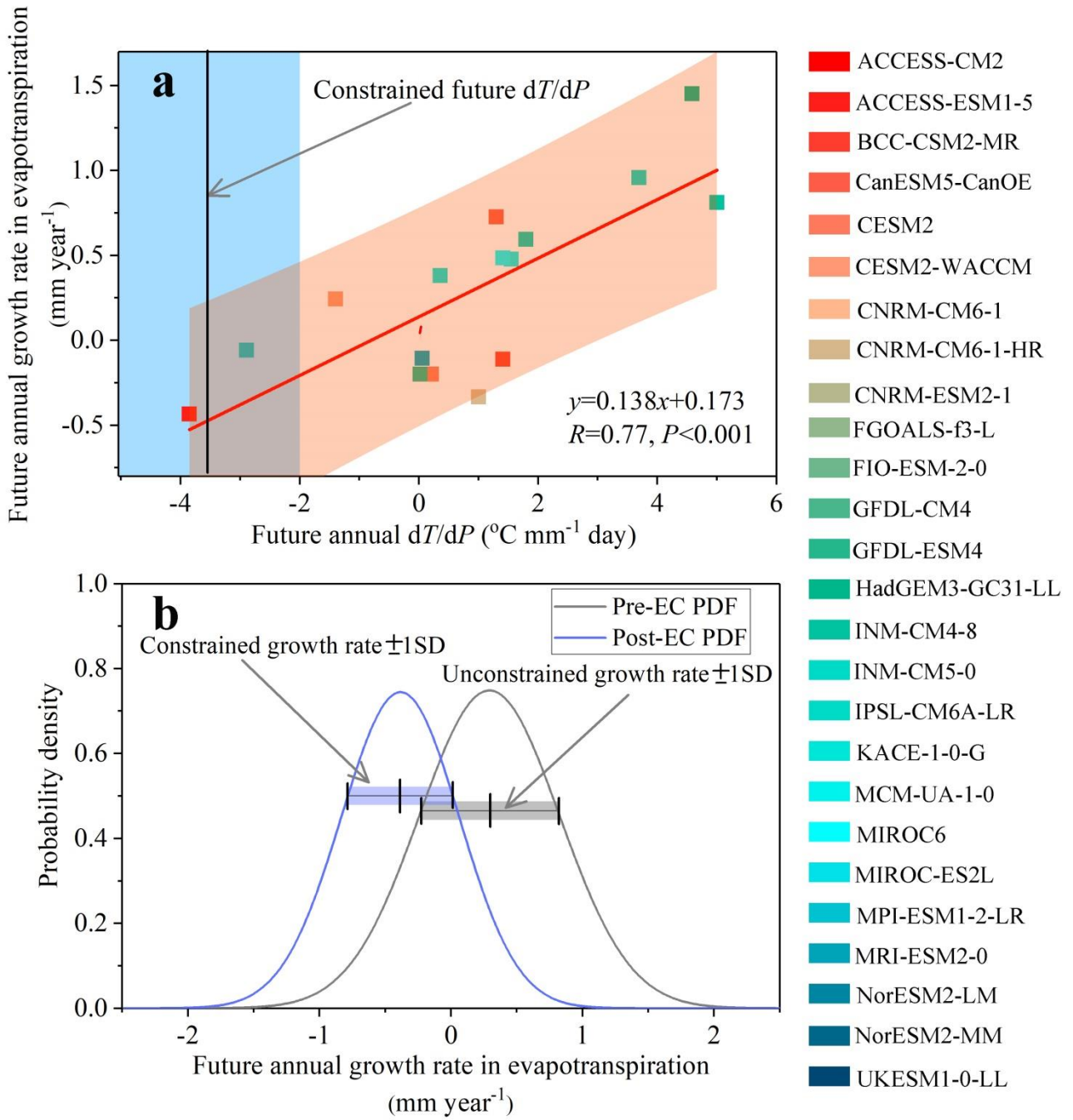
544

545 **Fig. 2**



546

547



549

550

